Non-Contact Thermal Conductivity Measurements of P-Doped and N-Doped Gold Covered Natural and Isotopically-Pure Silicon and their Oxides

Mihai G. BURZO, Pavel L. KOMAROV, and Peter E. RAAD
Department of Mechanical Engineering
Southern Methodist University
Dallas, TX 75275-0337, U.S.A.
praad@smu.edu, Tel +1-214-768-3866, Fax +1-214-768-4998

Abstract

The laser-based, non-contact, non-destructive transient thermo-reflectance (TTR) method was used to measure (i) the thermal conductivity of natural silicon and isotopically-pure silicon-28 layers that are epitaxially grown on natural silicon substrates; (ii) the thermal conductivity of the oxide of natural and isotopically-pure silicon; and (iii) the influence of doping type and level on the thermal conductivity at room temperature (300 K). The third study was carried out for low and higher levels of both phosphorous (p-type) and boron (n-type) doping. The results reveal that the thermal conductivity of silicon-28 oxide is equal to 1.43 W/m-K and is similar to the thermal conductivity reported for the oxide of natural silicon [1], i.e., 1.4 W/m-K. The data also shows consistent differences (~55%) in the thermal conductivity between natural and isotopically-pure Si, independently of the level of doping. Both the p and n-doping produce a decrease (~18%) in the thermal conductivity for both natural and isotopically-pure silicon. The thermal interface resistance between the top gold layer and the underlying epitaxial layer has also been measured and found to vary slightly from sample to sample.

1. Introduction

The high demand in modern consumer and industrial electronics has pushed the manufacturing of ICs to unforeseen scientific and technological limits. As manufacturers reach the spatial limits for the films that make up embedded elementary devices, the focus of R&D naturally shifts to finding new ways of improving the performance, reliability, and cost of new electronics besides shrinking the physical limits of a device. Some have looked into nanotechnology, which provides new ways of controlling the properties of materials and even producing “wonder materials” such are quantum dots discovered in the 70s by Alex Ekimov or nanotubes first manufactured by Roger Bacon in the early 1960s and observed for the first time through an electron microscope by Sumio Iijima in 1992 [2]. However, present manufacturing costs and technological limitations keep nanotechnology out of the realm of industrial scale fabrication. A more feasible alternative for improving electronic devices has been to develop new materials or modify existing materials and use them in the new chips. As an example, not long ago the entire computer processor manufacturing industry switched from using silicon to using silicon-germanium as the base semiconductor. It is therefore hoped that significant gains can also be made by the introduction of advanced materials such are isotopically pure materials considered in the present work.

The knowledge of thermophysical properties of materials used in the electronics industry plays a crucial role in the design process of electronic device and integrated circuits, especially for electronic and telecommunication devices, where performance depends heavily on electrothermal interactions. Higher performance is only possible by significant reductions in the size of active features, which in turn can increase heat generation densities to critical levels. With the use of submicron devices came the realization that bulk and thin-film thermal properties differ markedly [3]. However, since no universal behavior is expected for these differences and since they cannot be predicted from theory [4], the properties of each material must be measured separately. Also, as films are typically layered and deposition techniques differ by manufacturer, it is important to measure the interface resistance of stacked layers [5].

In nature, every element has a particular arrangement of protons and neutrons, called a favored isotope; e.g., silicon-28 is the favored isotope of silicon and has a nucleus that comprises of 14 protons and 14 neutrons. Silicon is composed of three stable isotopes (Si has eight possible isotopes in total, ranging from 24 to 34), namely, silicon-28 (92% natural abundance), silicon-29 (4.7%), and silicon-30 (3.3%). By purification at the sub-atomic level, it is possible to remove essentially all of the silicon-29 and silicon-30 leaving isotopically pure silicon-28, which has a more perfect crystalline lattice. This more perfect crystalline structure exhibits reduced phonon-phonon and phonon-electron interactions, which increases certain transport properties, such as thermal conductivity.

The anticipated advantages of using silicon-28 in manufacturing electronic devices include improved device performance (higher speed switching, smaller die sizes), higher reliability devices (fewer hot spots, lower temperatures at active junctions), improved yields (increased number of high speed chips) and less cooling required (smaller/cheaper packaging possible). Another advantage is that isotopically pure silicon-28 is chemically identical to natural silicon. Meaning, wafers made from silicon-28 can be processed using the same equipment and procedures as normal silicon wafers.

Previous works [6, 7] have shown that isotopically pure silicon-28 has close to 60% better room temperature thermal conductivity than natural silicon with its three isotopes. Certainly, improvements in other physical properties, such are electrical properties, are also theoretically possible.

Newer materials, such as silicon-28 and silicon-28 oxide, present an initial hurdle to the measurement of their thermal properties by methods such as the Transient Thermoreflectance (TTR) method because of the poor availability in the open literature of required material properties. But even when available, TTR measurements of the thermal conductivity can still be hindered by less-than-desirable optical properties of the top layer material (i.e., low thermo-reflection coefficient, low reflectivity, high transparency, surface roughness), which degrade the measurement performance of a given system. More specifically, dielectric materials such is silicon oxide have a low value of the extinction coefficient, k, which means that it is transparent for the irradiation of a heating laser. If the light penetration depth of the irradiation is larger than the layer thickness, the laser light cannot heat the layer under test, and thus the TTR method does not work. The next important problem is associated with the value of the thermoreflectance coefficient of the top layer material. That coefficient defines a rate of change in the reflectivity as a function of the temperature deviation of the sample surface. This coefficient needs to be sufficiently high in order to obtain an appropriate signal-to-noise ratio in the measurements. Usually, it must be higher than 10^{-5} per Kelvin. In addition to the requirement for the thermoreflectance coefficient, the range of linearity between changes in reflectivity and changes in temperature has to include the range of transient temperatures experienced by the surface during the measurements. Otherwise, nonlinear effects could entirely distort the transient temperature response of a sample during analysis. Another difficulty connected with optical properties of the top layer is the changing of the optical properties with time due either to long-term oxidization at room temperature or to accelerated oxidization at the higher temperatures experienced during laser irradiation pulsing. These chemical modifications of the top layer add uncertainty to the measurement procedure since they are not easily quantifiable.

In order to eliminate these difficulties, investigators have resorted to the use of a so-called metal “absorption” layer on top of the material under test (for instance Au in [8], and Al in [5]). Metal films are used because they exhibit high absorptivity and their optical properties are usually well known. Although, the use of other metals as an absorption layer has not been widely considered in order to determine which of them may be optimal absorption layers for covering a film material under test, gold seems to be a particularly attractive material for use as an absorption film because of good stability in its refractive indexes (n and k) in a normal laboratory environment, linear dependence between reflectivity and temperature changes in the range of up to 200 K, and sufficiently high thermoreflectance coefficient. For that reason, all of the samples investigate here were covered with a layer of Au. When possible, the thickness of the cover layer was optimized for best responsivity (lowest uncertainties) using our previous investigations [9, 10].

The main objectives of this work are to investigate the thermal properties of the oxide of isotopically pure silicon (silicon-28) and to assess the influence of doping type and level on the thermal conductivity of both silicon and silicon-28. Additional objectives are to corroborate the gains in thermal conductivity reported by Capinski et al. [6] for isotopically-pure Si.

2. Experimental and numerical methodologies

The experimental system used to obtain the transient thermo-reflectance (TTR) measurements in the SMU Nanoscale Electro-Thermal Sciences Laboratory (NETSL) is shown in Figure 1. The heating source is an Nd:YAG pulsed laser with 30 Hz repetition rate, 532 nm wavelength, 6.1 ns pulse duration and up to 0.5 mJ pulse energy (limited by the fiber optic cable). The irradiation pulse that heats the sample passes through the beam splitters, the beam shaping lens, and the microscope objective lens. A power meter can be used to read the level of heating energy delivered to the surface of a sample. Measurements have shown good uniformity of the heating spot, described by the Gaussian temporal distribution,

$$I(t) = \frac{2F}{\tau\sqrt{\pi}} e^{-4\left(\frac{t-t_0}{\tau}\right)^2} \qquad (1)$$

where F is the fluence of laser irradiation, t_0 is the time when the intensity reaches its maximum value, and τ is the duration of the laser pulse.

The probing light source is a HeNe CW laser with 632 nm wavelength, and linearly polarized single mode irradiation beam. A 5 m, polarization-preserving fiber optic cable with TEM_{00} mode delivers the probing irradiation to the assembly. The laser beam then passes through a beamsplitter and dichroic mirror. After that, the beam is focused by the microscope objective lens on the sample surface at the same area where the heating spot is located. Reflected from the heated sample surface, the probing beam returns by the same path, and is delivered by a fiber optic assembly to the sensitive area of a preamplified silicon PIN photodiode with a 1 ns maximum rise time. The intensity of the reflected light depends on the sample surface reflectivity, which is a function of the surface temperature. In order to measure the transient temperature response resulting from a heating energy pulse, the photodiode output signal is acquired by a computer using an integrated PCI-slot Gage oscilloscope card with 5 Giga-Samples per second data acquisition rate.

The sample and the positioning of the laser beams on its surface are viewed through an objective lens and a computer controlled compact CCD camera. The camera also provides a view of the sample area under test on the computer screen, using the LabView based GUI, and

makes it possible to adjust the heating and probing spot positions on the sample with micron resolution. The GUI has a reticle that can be used to measure features on the samples with micron resolution. The heating and probing spot dimensions for the 20X objective lenses used for these measurements are around 200 µm and 15 µm, respectively. The sample is positioned on a small translation stage that can be moved with a 0.5 µm resolution by the use of a three-dimensional traversing mechanism. This construction is designed for focusing and precise target positioning along the sample.

The governing mathematical equation used to model the transient thermal process in the sample is the usual heat conduction equation:

$$\rho\, C_p \left(\frac{\partial T}{\partial t} \right) = \nabla \left(K\, \nabla T \right) + \dot{Q}_{(r,z,t)} \tag{2}$$

where K is the material thermal conductivity, C_p is the heat capacity, Q is the heat source term, and ρ is the material density. The laser light absorbed by the sample acts as a volumetric heat source, Q, which is function of both time and space within the heating radius r:

$$\dot{Q}_{(r,z,t)} = \left(\frac{2\,F}{\tau \sqrt{\pi}} \right) e^{-4\left(\frac{t-t_0}{\tau} \right)^2} \left(1-R\right) \gamma\, e^{-\gamma z} \tag{3}$$

where F is the fluence of the laser, τ is the pulse duration width, t_0 is the time of the pulse peak, R is the reflectivity of the top layer, and γ is the absorption coefficient of the top layer.

An analytical solution has been developed for a single layer of material. However, for multi-layered structures, an analytical solution is either very difficult or even impossible to obtain. Therefore, a computer code was developed in order to solve the heat equation. The numerical approach has been verified with a grid convergence study and then validated against the analytical solution for a wafer made up of a single layer.

Because of the nature of the problem under consideration (heat spot, structure of the layer, etc.) cylindrical coordinates would normally be preferred. However, since the samples under study are isotropic in the θ-direction, the problem can be reduced to an axially-symmetric, two-dimensional domain. Further simplifications can be obtained by considering that the area of the heat spot is much larger than the probing spot area. In such cases, it is possible to solve a much simpler, one-dimensional problem. The fact that the problem can be considered one-dimensional has been confirmed by preliminary computations (the results obtained with 1D and 3D cylindrical coordinates show good agreement). The initial condition is constant room temperature, and the boundary conditions are adiabatic on the top surface of the sample and ambient isothermal on the bottom (295 K).

The heat equation is then discretized with central finite differences. Next, a factored implicit scheme (Beam and Warming) is implemented in order to solve the finite difference equations. Using this generalized time differentiation scheme, a wide choice of methods can be obtained (Euler implicit, Leapfrog explicit, trapezoidal, 3-pt-backward implicit, etc.) by selecting the proper values of two parameters. The three-point-backward scheme is used because of its higher accuracy and unconditional stability. This makes the algorithm second-order accurate in both space and time.

An elegant two-parameter optimization scheme is used to fit the experimental results with the numerically

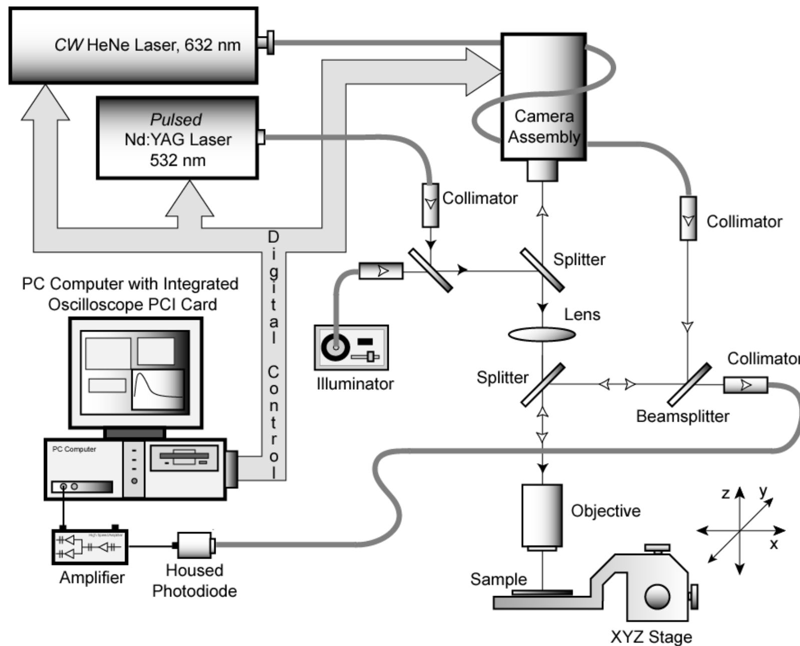

Figure 1 Schematic of the TTR experimental system

obtained transient response. The heat conduction equation (2) is solved for different values of thermal conductivity and thermal interface resistance (between the Au and the underlying layer) until the error between the numerical and experimental data is minimized in the RMS sense. This procedure makes it possible to obtain not only the thermal conductivity of the material under test, but also the thermal interface resistance existing between the absorption layer and the underlying material. Käding et al. [11] showed that the value of the interface resistance can be significant.

3. Results

Nine 4-inch, 635 μm-thick, silicon wafers with a 5 μm-thick epitaxial layer of either natural silicon or isotopically-pure silicon-28 (Table 1) were considered in this investigation. A layer of oxide was thermally grown on one of the natural Si and one of the Si^{28} samples. The thickness of the oxide layer is around 3 μm thick. All samples were covered by a gold layer, which serves the purpose of absorbing the laser power as well as keeping the surface optical properties of the samples identical [9]. The thickness of the gold layers was carefully measured by the use of a Dektak[3]ST profiler and is given in Table 1. In addition, to ensure that the optical properties are in fact the same as the values provided in the open literature, n and k of the Au cover were measured with a Gaertner L116S ellipsometer. The measured values of the optical parameters (the real and imaginary part of the refractive indices) are n = 0.41 and k = 2.45. The published values from the literature, n = 0.46 and k = 2.41 [12], are close to those measured in this work. In reality, the only optical parameter that will influence the results of the TTR measurement is the extinction coefficient, k. The value of the coefficient n, in conjunction with the fluence of the heating laser, will produce the peak temperature of the TTR transient response. Since the data is normalized anyway, the value of the peak is of no significance for the TTR measurements. As shown above, the difference between the measured data and the values found in the literature is very small, showing that the Au surface is of excellent optical quality. The above-mentioned difference yields less than 1% uncertainty in the thermal conductivity results. Nevertheless, the decision was made to use the values measured in our lab (n = 0.41 and k = 2.45).

The temperature data points obtained for sample 1 are plotted in Figure 2 along with the curve representing the best fit from the numerical solution of Eq. 2 for that sample. As previously mentioned, the aim of the fitting procedure is to determine both the thermal conductivity of the epitaxial material and the thermal interface resistance between the epitaxial and gold layers by minimizing the RMS error between the measured response and the numerical solution. If the measurement system were not capable of capturing the thermal physics correctly over the full width of the measurement time window (~200 ns), the raw data points would not have fallen on top of the curve as closely as is evident in Figure 2. Hence, the excellent agreement between the raw measurement data and the numerical solution is indicative of the quality of the measurement system.

Table 1 Thermal conductivity and interface resistance measurements for the samples investigated

Sample No.	Measuring Layer			Gold Cover (Å)	K ± σ% (W/m-K)	R_{th} ×10^9 ± σ% (m^2-K/W)
	Type	Doping Type	Doping Level			
1	Natural Si	Boron (N)	Low ($1\cdot10^{16}$)	4,070 ± 25	148 ± 5.8%	7.4 ± 3.3%
2	Natural Si	Boron (N)	High ($2\cdot10^{19}$)	4,010 ± 25	122 ± 6.1%	6.5 ± 14.1%
3	Si^{28}	Boron (N)	Low ($1\cdot10^{16}$)	5,130 ± 25	227 ± 5.7%	5.5 ± 6.8%
4	Si^{28}	Boron (N)	High ($2\cdot10^{19}$)	5,010 ± 25	190 ± 5.0%	5.5 ± 10.3%
5	Natural Si	Phosphorus (P)	High ($2\cdot10^{19}$)	5,040 ± 25	125 ± 3.8%	5.8 ± 7.9%
6	Si^{28}	Phosphorus (P)	High ($2\cdot10^{19}$)	5,120 ± 25	194 ± 6.5%	5.6 ± 4.2%
7	Natural Si	Phosphorus (P)	Low ($3\cdot10^{13}$)	4,960 ± 25	150 ± 3.1%	10.6 ± 3.4%
8	SiO_2	-	Undoped	5,200 ± 25	1.4± 5.0%	N/A
9	$Si^{28}O_2$	-	Undoped	4,930 ± 25	1.43 ± 5.0%	N/A

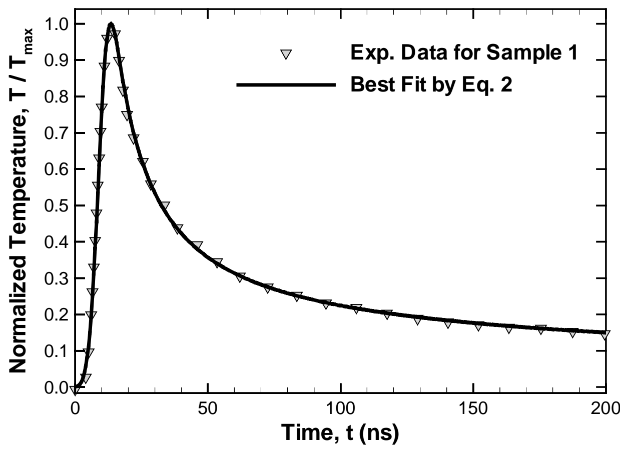

Figure 2 Experimental and numerically computed, normalized temperature response of epitaxially grown boron doped natural Si covered by gold (Sample 1)

The measured values of the thermal conductivity for the epitaxial material and the thermal interface resistance between the gold and epitaxial layers for the nine samples are presented in the two rightmost columns of Table 1, along with the associated percentage uncertainty values. The uncertainty values for each boron-doped sample are obtained by calculating the standard deviation of ten measurement trials, each consisting of 100 measured temperature responses at the same physical location. The uncertainty values for the phosphorous-doped samples are obtained by calculating the standard deviation of twenty-five measurement trials, each consisting of 1,000 measured temperature responses at the same physical location. The uncertainty values for the oxide covered sample are obtained by calculating the standard deviation of twenty measurement trials, each consisting of 2,000 measured temperature responses at the same physical location. The average uncertainty in the thermal conductivity is around 5%, while for the interface resistance, the average uncertainty is around 7%.

The measured values of K = 148 W/m-K for sample 1 and K = 150 W/m-K for sample 7 (Table 1) fall within the usual range of values reported for low doped natural Si. Since the values of the boron doped samples were discussed in our previous work [7], the present work will only focus on the results for the phosphorous doped and oxide covered samples. The values of the thermal conductivity and interface resistance for the p-doped samples that are shown in Table 1 were calculated by averaging the data obtained in 25 different locations along each sample, and using 2,000 trials at each location. As a result, the uncertainty of the measurement is kept at very low values. This was mainly possible because of the second-generation TTR system that is almost two orders of magnitude faster than the previous system. The thermal conductivity results for samples 5, 6, and 7 are plotted in Figure 3 while the corresponding interface thermal resistance results are shown in Figure 4.

Analyzing the data shown in Table 1, one is able to compare the effects of (i) isotopic purity as well as (ii) dopant type and (iii) dopant level on the thermal conductivity and interface resistance. To facilitate the comparison, the effect of each of the above three factors is shown as a percentage change in Tables 2-4. Thus, in Table 2 we present the effect of isotopic purity on the measured thermal conductivity. As observed from examining the last column of Table 2, sample 3 shows a 54% gain in the thermal conductivity at room temperature, as compared with sample 1, indicating that n-doped isotopically-pure silicon (Si^{28}) is appreciably more thermally conductive than n-doped natural silicon. Comparing the results of the higher doped samples (2 and 4) reveals that the thermal conductivity of sample 4 (Si^{28}) is 56% higher than that of sample 2 (Si). A 55% increase was also observed in the case of p-doped Si^{28} sample (sample 5) as compared to the p-doped natural Si sample (sample 6). This level of gain is close to the gain observed between the lower doped silicon samples 2 and 4 and samples 1 and 3. This consistency provides a level of confidence that Si^{28} is notably more conductive than natural Si, at the lower as well as at the higher levels of doping, for both n-type and p-type doping. The difference between the natural and isotopically pure silicon is slightly higher (2%) for the samples doped with higher concentrations of boron or phosphorous than for the samples doped with a low level

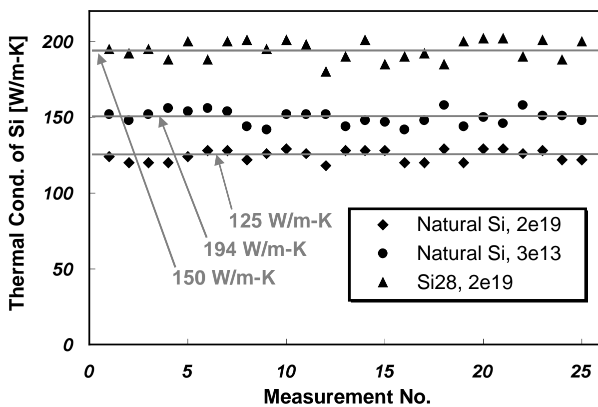

Figure 3 Thermal Conductivity measurements of phosphorous doped samples (Samples 5, 6, and 7)

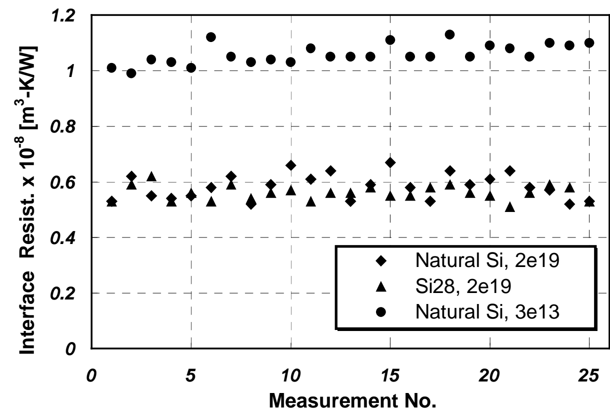

Figure 4 Interface thermal resistance measurements of phosphorous doped samples (Samples 5, 6, and 7)

Table 2 Effect of isotopic purity on the thermal conductivity of n(boron) and p(phosphorous)-doped natural and isotopically pure silicon samples.

Compared Samples	Description of the samples comparison		Mathematical Expression	Change in K (%)
	Sample	Compared To		
1 & 3	Low n-doped *Natural Si*	Low n-doped *Natural* Si^{28}	$(K_3-K_1)/K_1$	54%
2 & 4	High n-doped *Natural Si*	High n-doped Natural Si^{28}	$(K_4-K_2)/K_2$	56%
5 & 6	High p-doped *Natural Si*	High p-doped Natural Si^{28}	$(K_6-K_5)/K_5$	55%

of boron. However, this difference is within the uncertainty of the measurements.

The effect of doping level on the thermal conductivity of the samples can be identified by examining the results in Table 3. Sample 2 (higher n-doped Si) shows a 18% decrease in the thermal conductivity as compared to sample 1 (lower n-doped Si), which is due to the different level of boron doping in sample 2. Similarly, sample 4 exhibits a 20% drop in the thermal conductivity as compared to the more highly doped sample 3. Since again the only difference between the two samples is the doping level, the drop in conductivity is attributable to the higher doping level of sample 4. A similar behavior is observed for the p-doped sample. Namely, sample 5 (higher p-doped Si) shows a 17% decrease in the thermal conductivity as compared to sample 7. The effect of doping on the thermal conductivity of Si^{28} is very close to that observed with both the p-doped and n-doped natural Si samples.

The effect of the doping *type* on the thermal conductivity of samples investigated here is presented in Table 4. As evident form the last column of Table 4, the differences are undetectable (smaller than the uncertainty of the TTR measurements). Thus, we can conclude that both the qualitative and quantitative behavior of the n-type and p-type dopants on the thermal conductivity is identical.

The overall data reveal consistent differences (~55%) in the thermal conductivity between natural and isotopically-pure Si, independently of the level and type of doping. The 55% gain is close to the 60% gain at room temperature reported by Capinski et al. [6] for intrinsically doped Si. From the current work, it can also be seen that the effects of isotopic purity and doping level are independent of each other. The loss in thermal conductivity of around 18% due to higher doping is smaller than that reported in reference [13] (~34%); however, the qualitative behavior of the results obtained in this work is consistent. A possible explanation for this discrepancy is the dependence of the specific heat (ρC_p) on the doping level. Since the numerical technique used to deduce the thermal conductivity requires (ρC_p) as an input parameter, uncertainties in the specific heat can result in errors in the calculated thermal conductivity. Unfortunately, the dependence of ρC_p on doping level and isotopic purity has not yet received attention in the open literature and remains an undeveloped issue.

The thermal interface resistance between the top gold layer and the underlying epitaxial layer appears to vary slightly from sample to sample. The range of the measured values falls within the envelope of the resistance reported by Käding et al. [11], namely, 0.8×10^{-8} to 4.3×10^{-8} m^2-K/W, indicating that the adhesion of the gold layer to the epitaxial material is very good. The interface between the epitaxially grown layer and the underlying Si wafer plays no role in the analysis since the epitaxial layer is thicker than the heat penetration depth during a complete measurement cycle. In other words, the ~500 ns duration of the cycle is not long enough for the heat front

Table 3 Effect of doping level on the thermal conductivity of n(boron) and p(phosphorous)-doped natural and isotopically pure silicon samples

Compared Samples	Description		Mathematical Expression	Change in K (%)
	Sample	Compared To		
1 & 2	*Low* n-doped Natural Si	*High* n-doped Natural Si	$(K_2-K_1)/K_1$	-18%
3 & 4	*Low* n-doped Si^{28}	*High* n-doped Si^{28}	$(K_4-K_3)/K_3$	-20%
7 & 5	*Low* p-doped Natural Si	*High* p-doped Natural Si	$(K_5-K_7)/K_7$	-17%

Table 4 Effect of doping type on the thermal conductivity of n(boron) and p(phosphorous)-doped natural and isotopically pure silicon samples

Compared Samples	Description		Mathematical Expression	Change in K‡ (%)
	Sample	Compared To		
1 & 7	Low *n-doped* Natural Si	Low *p-doped* Natural Si	$(K_7-K_1)/K_1$	1.4%
2 & 5	High *n-doped* Natural Si	High *p-doped* Natural Si	$(K_5-K_2)/K_2$	2.5%
4 & 6	High *n-doped* Si^{28}	High *p-doped* Si^{28}	$(K_6-K_4)/K_4$	2.1%

‡ Note: Changes are undetectable since they are smaller than the uncertainty of the TTR measurements

to interact with the interface between the epitaxial layer and the underlying Si wafer.

We also performed and present here measurements of the thermal conductivity of the oxide of Si^{28}, which to the authors' knowledge is the first time that such a study has been reported. The thickness of the grown oxide layer was measured and found to be larger than the minimum thickness at which a sample can be considered bulk from the TTR measurements point of view (1.04 μm for the SMU system). Tests were performed at twenty different points on the gold covered Si^{28} oxide sample with 2,000 measurements trials at each point. The measured value of thermal conductivity of Si^{28} oxide is shown in the last row of Table 2 and is 1.425 ± 5.0% W/m-K. The measured data is presented in Figure 5 at all of the twenty locations measured along the sample. The results reveal that the thermal conductivity of silicon-28 oxide is comparable (within the TTR measurement uncertainty) to the thermal conductivity reported for the oxide of natural silicon [1] (1.4 W/m-K).

4. Conclusions

The transient thermoreflectance method has been employed to measure for the first time (to the authors' knowledge) the room temperature thermal conductivity for the oxide of the silicon-28. Both the natural silicon oxide and silicon-28 oxide layers were thermally grown and their thickness was sufficiently high so that they could be considered bulk material from the point of view of TTR measurements. Thermal conductivity and interface thermal resistance measurements were also performed for seven n and p-doped natural and isotopically-pure silicon-28 samples, with both low and higher levels of doping of the epitaxial layers. For the p-doped samples the low level of phosphorous doping is 3×10^{13} atoms/cm^3 and the high level is 2×10^{19} atoms/cm^3. For the n-doped samples the low level of boron doping is 10^{16} atoms/cm^3 and the high level is 2×10^{19} atoms/cm^3.

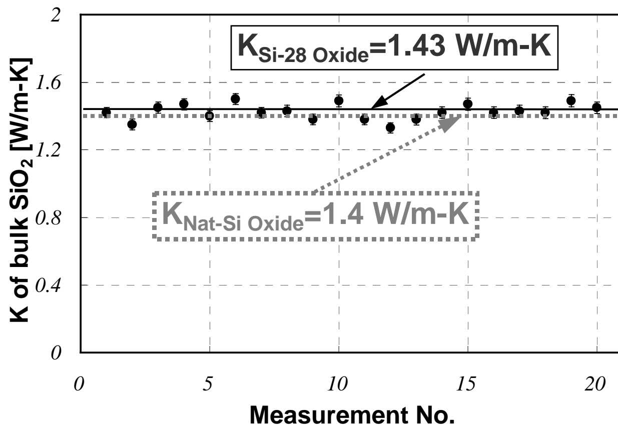

Figure 5 Thermal Conductivity measurements of the oxide of Si^{28}

The results reveal that the thermal conductivity of silicon-28 oxide is equal to 1.425 W/m-K and is similar to the thermal conductivity reported for the oxide of natural silicon [1] (within the TTR measurement uncertainty). The results indicate a gain of approximately 55% in the thermal conductivity of silicon-28 as compared to that of natural Si, at both low and higher levels of p and n-doping, and a decrease of approximately 18% in the thermal conductivity for both types of silicon due to the higher level of doping. It is worth mentioning that the 55% gain is close to the 60% gain at room temperature reported by Capinski et al. [6] and the first study by Ruf et al. [14] for isotopically-pure Si and is higher that the 10% gain reported in a later communication by Ruf et al. [15].

The thermal interface resistance between the top gold layer and the underlying epitaxial layer has also been measured and appears to vary slightly from sample to sample. The range of the measured values falls within the envelope of the resistance reported by other investigators (e.g., Käding et al. [11]), namely, 0.8×10^{-8} – 4.3×10^{-8} m^2-K/W, indicating that the adhesion of the gold layer to the epitaxial material is very good. The interface between the epitaxially grown layer and the underlying Si wafer plays no role in the analysis since the epitaxial layer is thicker than the heat penetration depth during a measurement cycle. The interface resistance for the measured oxide samples plays no role either since the oxide layer is much thicker than the heat penetration depth during the TTR measurements.

The results obtained in this work for the silicon-28 samples are in good agreement with the previous results of Capinski et al. [6], and provide additional evidence in support of the thermal advantage of Si^{28} (a gain of approximately 55% as compared to the thermal conductivity of natural silicon). For the range of doping investigated in this work, the change in the thermal conductivity is inversely proportional with the doping level, for both p-type and n-type doping. Nevertheless, no gain has been observed for the silicon-28 oxide layers as compared to the oxide of natural silicon. This result is expected since the oxide layer is an amorphous material and no changes in the structure of the material are expected as compared to pure silicon, where the other two isotopes produce a change in the structure of the sample.

Acknowledgments

The authors gratefully acknowledge Isonics Corp. of Golden, Colorado, for providing the research support to conduct this investigation. The authors are also thankful to Dr. Stephen Burden of Isonics for providing the required samples. The natural Si and boron doped silicon-28 samples were covered with gold by Dr. Howard Beratan and his Raytheon colleagues at the uncooled detector branch of Raytheon in Dallas, TX. The authors are grateful to Dr. Beratan and Raytheon for providing this support at no cost to this project. The oxide and phosphorous doped silicon-28 samples were covered with gold by Lance Goddard Associates (LGA Films).

References

1. Powell, R. W., Ho, C. Y., and Liley P. E., Thermal Conductivity of Selected Solids, NSRDS-NBS 8, Nov. 25, 1966
2. Iijima, S., Ajayan, P. M., and Ichihashi, T., "Growth model for carbon nanotubes," *Physical Review Letters*, Vol. 69, No. 21 (1992), p. 3100.
3. Tien, C. L., Majumdar A., and Gerner, F. M. (Eds.), Microscale Energy Transport, Taylor and Francis (Washington, DC, 1998).
4. Majumdar, A., "Microscale Heat Conduction in Dielectric Thin Films," *ASME Journal of Heat Transfer*, Vol. 115 (1993), pp. 7-16.
5. Capinski, W. S., and Maris, H. J., "Improved Apparatus for Picosecond Pump-and-probe Optical Measurements," Review of Scientific Instruments, Vol. 67, No. 8 (1996), pp. 2720-2726.
6. Capinski, W. S., Maris, H. J., Bauser, E., Silier, I., Asen-Palmer, M., Ruf, T., Cardona, M., and Gmelin, E., "Thermal conductivity of Isotopically Enriched Si," *Appl. Phys. Letters*, Vol. 71 (1997), p. 2109.
7. Komarov, P. L., Burzo, M. G., Kaytaz, G., and Raad, P. E., "Transient Thermo-Reflectance Measurements of the Thermal Conductivity and Interface Resistance of Metallized Natural and Isotopically-Pure Silicon," *Microelectronics Journal*, Vol. 34 (2003), pp. 115-118.
8. Paddock, A., Eesley, G. L., "Transient Thermoreflectance from Thin Metal Films," *J. Applied Physics*, Vol. 60, No. 1 (1986), pp. 285-290.
9. Burzo, M. G., Komarov, P. L., and Raad, P. E., "Influence of a Metallic Absorption Layer on the Quality of Thermal Conductivity Measurements by the Transient Thermo-Reflectance Method," *Microelectronics Journal*, Vol. 33 (2002), pp. 697-703.
10. Burzo, M. G., Komarov P. L., and Raad, P.E., "Minimizing the Uncertainties Associated with the Measurements of Thermal Properties by the Transient Thermo-Reflectance Method," *9th International IEEE Workshop on THERMal INvestigations of ICs and Systems (THERMINIC)*, Aix-en-Provence, France, Sep. 2003, pp. 257-262.
11. Käding, O. W., Skurk, H., and Goodson, K. E., "Thermal Conduction in Metallized Silicon-Dioxide Layers on Silicon," *Appl. Phys. Letters*, Vol. 65 (1994), p. 1629.
12. Palik, E.D. (Editor), Handbook of Optical Constants of Solids, Academic Press, (San Diego, CA 1998).
13. Asheghi, M., Kurabayashi, K., Goodson, K. E., Kasnavi, R., and Plummer, J.D., "Thermal Conduction in Doped Silicon Layers," *33rd ASME/AIChE National Heat Transfer Conference*, Albuquerque, NM, Aug. 8-14, 1999.
14. Ruf, T., Henn, R. W., Asen-Palmer, M., Gmelin, E., Cardona, M., Pohl, H.-J., Devyatych, G. G., and Sennikov, P. G., "Thermal Conductivity of Isotopically Enriched Silicon," *Solid State Comm.*, vol. 115, May (2000), pp. 243-247
15. Ruf, T., Henn, R. W., Asen-Palmer, M., Gmelin, E., Cardona, M., Pohl, H.-J., Devyatych, G. G., and Sennikov, P. G., Erratum to "Thermal Conductivity of Isotopically Enriched Silicon," *Solid State Communications*, vol. 127(2003), p. 257.